

1 Effect of land-sea air masses transport on spatiotemporal distributions of atmospheric CO<sub>2</sub>  
2 and CH<sub>4</sub> mixing ratios over the south Yellow Sea

3 Jiaxin Li <sup>1</sup>, Kunpeng Zang <sup>1,2,3\*</sup>, Yi Lin <sup>1</sup>, Yuanyuan Chen <sup>1</sup>, Shuo Liu <sup>1</sup>, Shanshan Qiu <sup>1</sup>, Kai Jiang  
4 <sup>1</sup>, Xuemei Qing <sup>1</sup>, Haoyu Xiong <sup>1</sup>, Haixiang Hong <sup>1</sup>, Shuangxi Fang <sup>2,4\*</sup>, Honghui Xu<sup>5</sup>, Yujun  
5 Jiang<sup>5</sup>

6 <sup>1</sup> College of Environmental and Resources Sciences, Zhejiang University of Technology,  
7 Hangzhou, China, <sup>2</sup> Zhejiang Carbon Neutral Innovation Institute, Zhejiang University of  
8 Technology, Hangzhou, China, <sup>3</sup> National Marine Environmental Monitoring Center, Dalian,  
9 China, <sup>4</sup> Collaborative Innovation Center on Forecast and Evaluation of Meteorological Disasters  
10 (CIC-FEMD), Nanjing University of Information Science & Technology, Nanjing, China, <sup>5</sup>  
11 Zhejiang Meteorological Science Institute, Hangzhou, China

12 **Corresponding to:** Kunpeng Zang ([zangkunpeng@zjut.edu.cn](mailto:zangkunpeng@zjut.edu.cn)), Shuangxi Fang  
13 ([fangsx@zjut.edu.cn](mailto:fangsx@zjut.edu.cn))

14  
15 **Abstract:** To reveal the spatiotemporal distributions of atmospheric CO<sub>2</sub> and CH<sub>4</sub> mixing ratios  
16 and regulation mechanisms over the China shelf sea, two field surveys were conducted in the  
17 south Yellow Sea in China in November 2012 and June 2013, respectively. Observed results  
18 showed that mean background atmospheric CO<sub>2</sub> and CH<sub>4</sub> mixing ratios were 403.94 (13.77) ppm  
19 and 1924.8 (27.8) ppb in November 2012, and 395.90 (3.53) ppm and 1918.0 (25.7) ppb in June  
20 2013, respectively. An improved data filtering method was optimized and established to flag  
21 atmospheric CO<sub>2</sub> and CH<sub>4</sub> emission from different sources in survey area. We found that, the  
22 spatiotemporal distributions of atmospheric CO<sub>2</sub> and CH<sub>4</sub> mixing ratios over the south Yellow Sea  
23 were dominated by land-sea air masses transport, which was mainly driven by seasonal monsoon,  
24 while the influence of air-sea exchange was negligible. In addition, atmospheric CO<sub>2</sub> and CH<sub>4</sub>  
25 mixing ratios over the south Yellow Sea could be elevated remarkably in a distance of  
26 approximate 20 km offshore by land-to-sea air masses transportation from the Asia Continent

1 during early winter monsoon.

2 **Keywords:** carbon dioxide, methane, monsoon, marine boundary air, shipborne underway  
3 measurement.

#### 4 1 Introduction

5 Carbon dioxide (CO<sub>2</sub>) and methane (CH<sub>4</sub>) are the two most important greenhouse gases,  
6 playing critical roles in Earth's radiation balance (AGGI, 2014; WMO greenhouse gas bulletin,  
7 2022). Since the industrial revolution era (~1750), atmospheric CO<sub>2</sub> and CH<sub>4</sub> mixing ratios have  
8 been increasing, and reached their highest values of  $415.7 \pm 0.1$  ppm and  $1908 \pm 2$  ppb in 2021,  
9 which were about 149% and 262% of the preindustrial levels (WMO greenhouse gas bulletin,  
10 2022). Increasing of atmospheric CO<sub>2</sub> and CH<sub>4</sub> was unequivocally attributed to anthropogenic  
11 emissions, e.g., industrial production, deforestation, fossil fuel consumption (Houghton, 2003;  
12 Peters et al., 2012), and natural source-sink processes (Zang et al., 2017).

13 For decades, spatiotemporal distributions of atmospheric CO<sub>2</sub> and CH<sub>4</sub> mixing ratios have  
14 attracted more and more attention from science community. Shipborne observation was considered  
15 as one of six common and important methods for observing greenhouse gases (Matsueda et al.,  
16 1996; Daube et al., 2002; Dlugokencky et al., 2005; Crosson, 2008; Fang et al., 2015). Based on  
17 shipborne discrete sampling and measurement, latitudinal distribution of CH<sub>4</sub> mixing ratio with a  
18 sharp drop in the area of 20 °N in marine boundary air of the North Pacific Ocean were reported,  
19 which was mainly influenced by air masses transportation driven by both winter monsoon and  
20 trade wind (Matsueda et al., 1996; Dlugokencky et al., 2005). In coastal area of the Bohai Sea,  
21 seasonal variations of atmospheric CO<sub>2</sub>, CH<sub>4</sub> and N<sub>2</sub>O mixing ratios were mainly influenced by  
22 land-sea air masses transportation based on discrete sampling observation (Kong et al., 2010).  
23 Moreover, periodic observed CO<sub>2</sub> and CH<sub>4</sub> mixing ratios in marine boundary air were also used to  
24 improve the accuracy of calculated air-sea CO<sub>2</sub> flux in the northern South China Sea and the  
25 Luzon Strait (Zhai et al., 2015), and assess impacts of several episodic oil and gas spill events on  
26 abnormal air-sea CH<sub>4</sub> flux in the Bohai Sea (Zhang et al., 2014).

27 In recent years, high-accuracy and high-resolution shipborne continuous observation method  
28 has been developed and applied to observe greenhouse gases in marine boundary air (Nara et al.,  
29 2014; Zang et al., 2017; Reddick et al., 2019), which could reveal more detailed information

1 associated with their source-sink processes. Latitudinal distributions of both CO<sub>2</sub> and CH<sub>4</sub> mixing  
2 ratios in the China shelf sea boundary air in early spring were observed, which were similar to that  
3 in the north Pacific Ocean (Matsueda et al., 1996; Zang et al., 2017), and mainly impacted by  
4 atmospheric chemical processes, air-sea interaction in Yangtze River estuary area and land-sea air  
5 masses transportation (Zang et al., 2017; Liu et al., 2018). Meanwhile, peak values of CO<sub>2</sub> and  
6 CH<sub>4</sub> mixing ratios in downwind area of offshore oil and gas platforms, which were recognized as  
7 hot spot sources of greenhouse gases, were observed by shipborne continuously measurement  
8 systems in the North Sea, the South China Sea and Bohai Sea. Combined with the Gaussian plume  
9 model, CH<sub>4</sub> emissions could be quantified via “top-down” approach (Nara et al., 2014; Riddick et  
10 al., 2019; Zang et al., 2020).

11 Monsoon is a kind of climatic phenomenon in which the dominant wind system changes with  
12 seasons (Lyu et al., 2021). The East Asian monsoon (EAM), comprising the East Asian summer  
13 monsoon (EASM) and East Asian winter monsoon (EAWM), is an important component of the  
14 Earth’s climate system and significantly influences the socioeconomic, agricultural and cultural  
15 development of East Asia (Huang, 1985; Zou et al., 2018; Lyu, et al., 2021). Previous studies have  
16 shown that the East Asian monsoon played an important role in global and regional climate  
17 variability (Huang, 1985; Chang et al., 2000; Ding et al., 2007; Zhan and Li, 2008). On the one  
18 hand, spatiotemporal distributions of CO<sub>2</sub> and CH<sub>4</sub> in marine boundary air were influenced by  
19 multiple processes, such as land-sea air masses transport (Bartlett et al., 2003; Zang et al., 2017),  
20 ship emission (Warneke et al., 2005; Law et al., 2013; Bouman et al., 2017; Ding et al., 2018)  
21 and oil and gas platforms (Nara et al., 2014; Reddick et al., 2019; Zang et al., 2020). On the other  
22 hand, greenhouse gases have been observed and studied in East Asia and Pacific Ocean based on  
23 land (island)-based stations (Fang et al., 2015; 2017; Luan et al., 2016), ship and plane observation  
24 platforms for many years (Matsueda et al., 1996; Bartlett et al., 2003; Dlugokencky et al., 2005).  
25 However, as an important pathway of atmospheric components transportation between the Asia  
26 Continent and Pacific Ocean, spatiotemporal distributions and regulation mechanisms of CO<sub>2</sub> and  
27 CH<sub>4</sub> in the China shelf seas boundary air were still rare (Zhang et al., 2007; Zang et al., 2017; Liu  
28 et al., 2018).

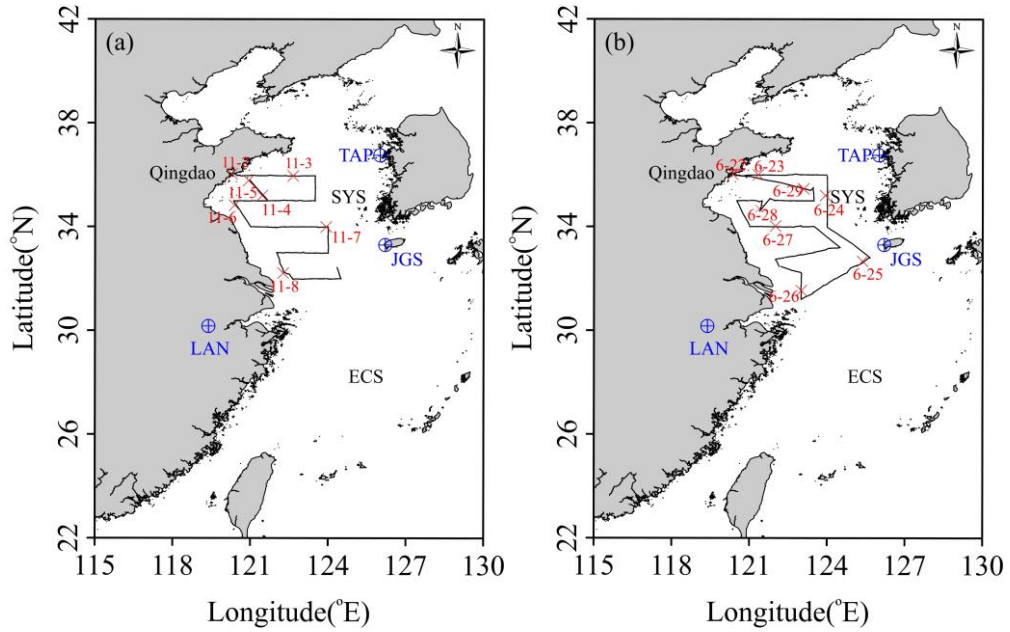
29 In this study, atmospheric CO<sub>2</sub> and CH<sub>4</sub> mixing ratios in boundary air of the South Yellow

1 Sea (SYS) were simultaneously observed by a self-assembled shipborne CRDS (Cavity Ring-  
2 down Spectroscopy, Picarro G2301, USA) system in November 2012 and June 2013, when typical  
3 periods of the EASM and the EAWM. The major objectives of this work were (1) to optimize an  
4 improved data filter approach for shipborne continuous mobile observation of atmospheric CO<sub>2</sub>  
5 and CH<sub>4</sub> mixing ratios, (2) to investigate the influence of air-sea exchange on the spatiotemporal  
6 distributions of CO<sub>2</sub> and CH<sub>4</sub> mixing ratios, and (3) to reveal the regulating mechanisms of  
7 seasonal monsoon on spatiotemporal distributions of CO<sub>2</sub> and CH<sub>4</sub> in marine boundary air of the  
8 SYS during the field surveys.

## 9 2 Method and materials

### 10 2.1 Observation area

11 The Yellow Sea is a semi-enclosed marginal sea, located on the western part of the Pacific  
12 Ocean, adjacent by China to the north and west, and Korean Peninsula to the east (Zhang and Chu,  
13 2018; Wang et al., 2021). It is a main pathway of air mass transport between the Asia continent  
14 and Pacific Ocean, and can be divided into two basins: the North Yellow Sea (NYS) and the SYS  
15 (Lyu et al., 2021). The SYS covers an area of about  $10.8 \times 10^4$  km<sup>2</sup>, with an average depth of 44 m,  
16 and is strongly influenced by the EAM system (Zou et al., 2018). As showed in Fig. 1, to study the  
17 distributions of atmospheric CO<sub>2</sub> and CH<sub>4</sub> mixing ratios and their regulation mechanisms, two  
18 campaigns were conducted from 2<sup>nd</sup> to 8<sup>th</sup> November, 2012 and from 22<sup>nd</sup> to 29<sup>th</sup> June, 2013,  
19 respectively, when the typical periods of the EAM (including summer monsoon and winter  
20 monsoon). In order to ensure the comparability of observations, parallel observed CO<sub>2</sub> and CH<sub>4</sub>  
21 data from the three land (island)-based stations (LAN, JGS, TAP) located in vicinity area, were  
22 presented and studied in this study.



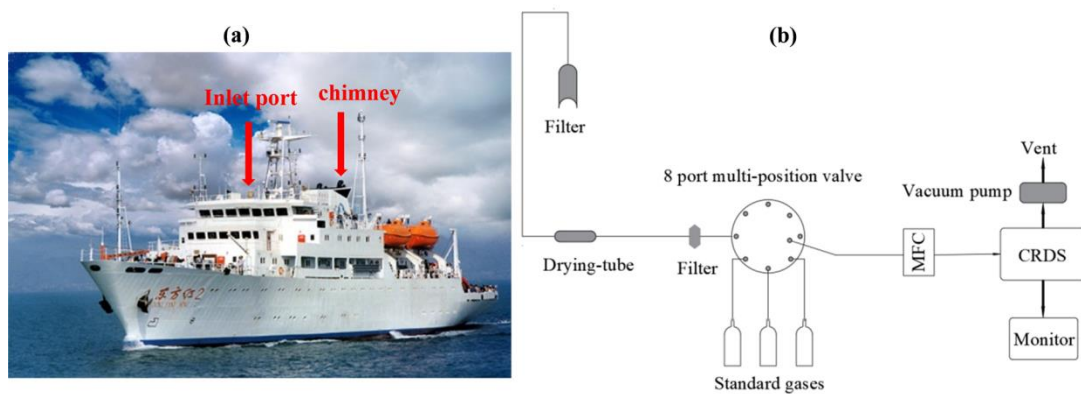
1  
 2 Fig. 1. Observation area in the SYS. The thick solid black lines represent cruise tracks in  
 3 November 2012 (a) and June 2013 (b). Symbols represent the Tae-ahn Peninsula station (TAP,  
 4 36.73 °N 126.13 °E, 20 m above sea surface), Jeju Gosan station (JGS, 33.30 °N 126.20 °E, 25 m  
 5 above sea surface) and Lin'an station (LAN, 30.18 °N 119.44 °E, 138 m above sea surface),  
 6 respectively ([https://www.esrl.noaa.gov/gmd/dv/site/site\\_table.html](https://www.esrl.noaa.gov/gmd/dv/site/site_table.html)). ECS represents the East  
 7 China Sea. The Red Crosses represent the beginning locations of each natural day.

8 2.2 Measurement of atmospheric CO<sub>2</sub> and CH<sub>4</sub> mixing ratios

9 As showed in Fig. 2a, during the field surveys, the air inlet was fixed at the highest point of  
 10 the bow, about 10 meters above the sea surface, and near the meteorological sensors for avoiding  
 11 anthropogenic contamination (Zang et al., 2017). Atmospheric CO<sub>2</sub> and CH<sub>4</sub> mixing ratios were  
 12 measured by using a self-assembled Picarro system (G2301, Picarro Inc., USA). The Picarro  
 13 analyzer, which can acquire one measurement every 5 seconds, and correct the measurements  
 14 influenced by water vapor (Rella et al., 2013), has been proven to be excellent for measuring CO<sub>2</sub>  
 15 and CH<sub>4</sub> with high precise and accuracy (Crosson, 2008; Fang et al., 2013).

16 As showed in Fig. 2b, ambient air was pumped via the dedicated tube by an external vacuum  
 17 pump, and passed through a membrane filter (1.0 μm, Whatman Inc., USA), a drying-tube filled  
 18 with magnesium perchlorate [Mg(ClO<sub>4</sub>)<sub>2</sub>] and another filter, respectively, to remove particles and  
 19 water vapor. Then, regulated by valve sequence setting, dry and clean air sample as well as the  
 20 standard gases flowed into the CRDS analyzer through 8 port multi-position valve (Valco

1 Instruments Co. Inc. USA) with a flow rate of  $200 \text{ mL} \cdot \text{min}^{-1}$  controlled by a mass flow controller  
2 (Beijing Seven-star electronics Co. LTD. China). Before and after each campaign, the CRDS  
3 analyzer was calibrated to guarantee its normal operation status. During field surveys, three  
4 standard gases were automatically measured in sequence each day, which was regulated by the  
5 CRDS analyzer. Linear functions were yielded based on measurement results and standard values  
6 of three standard gases, i.e., 254.53 (0.06) ppm, 365.14 (0.06) ppm and 569.99 (0.08) ppm for  
7  $\text{CO}_2$ , and 1601.0 (0.8) ppb, 1925.5 (0.8) ppb and 2317.7 (0.5) ppb for  $\text{CH}_4$ , respectively, which  
8 were used to calibrated the observed data. The used standard gases were propagated from the  
9 WMO primary standards (WMO/GAW 2004 scale for  $\text{CH}_4$ , 2007 scale for  $\text{CO}_2$ ), to guarantee the  
10 consistency, trace ability and international comparability of observed data (Dlugokencky et al.,  
11 2005).



12  
13 Fig. 2. The RV Dongfanghong II (a). Schematic diagram of the shipborne Picarro system for  
14 observing atmospheric  $\text{CO}_2$  and  $\text{CH}_4$  (b).

### 15 2.3 Meteorological data

16 Both of the two campaigns were conducted by a ship named “*Dongfanghong II*”, which was  
17 designed for multiple disciplines research in marine environment with a ship-based atmospheric  
18 science lab. Meteorological data, including time, latitude, longitude, cruising speed and direction,  
19 wind speed, wind direction, relative humidity, air pressure and temperature were observed by the  
20 meteorological sensors (RM Young, USA) with resolution of 10 seconds, and were used to filter  
21 and flag the observed  $\text{CO}_2$  and  $\text{CH}_4$  mixing ratios and verify simulated wind fields.

### 22 2.4 Air mass transport model

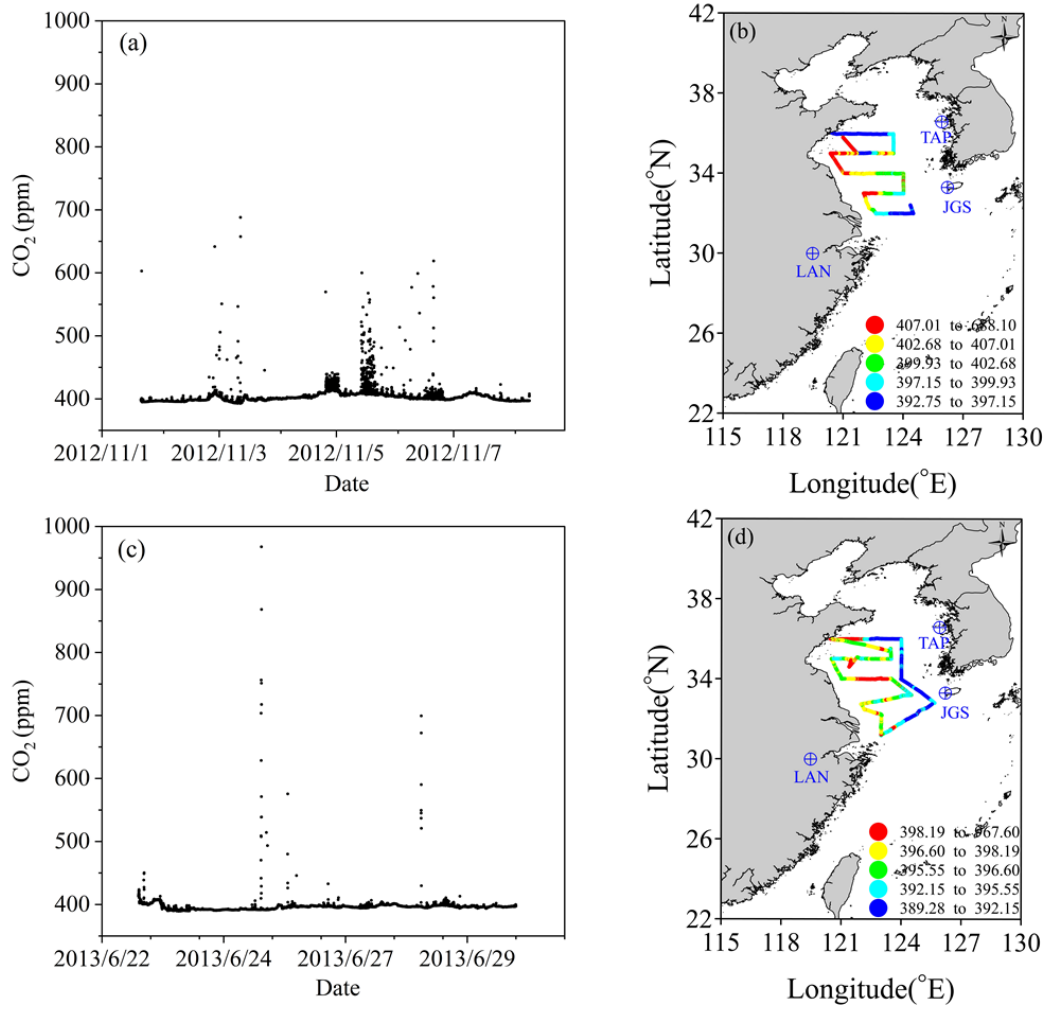
23 HYSPLIT ( Hybrid Single Particle Lagrangian Integrated Trajectory Model, HYSPLIT ) is  
24 developed by the National Oceanic and Atmospheric Administration's Air Resources Laboratory

1 (NOAA-ARL) and the Bureau of Meteorology of Australia, which can simulate the air mass  
2 transportation combined with the National Centers for Environmental Prediction (NCEP)  
3 reanalysis data. The principle of simulating the air mass transportation path is as follows:  
4 assuming that particles in the air are floating in the wind, their moving trajectory is the integral of  
5 their position vectors in time and space (Zhang et al., 2011; Xia et al., 2018). Backward trajectory  
6 analysis uses the mixed single-particle Lagrangian integral transport and diffusion model to  
7 calculate the air particles forward, analyzes the influence of air mass transportation on the spatial  
8 and temporal distribution of atmospheric components in the observation area by tracking the  
9 transport path, and infer their potential sources. The main parameters required to calculate the  
10 backward trajectory are the altitude, latitude and longitude of the starting point. Generally, the  
11 calculation is carried for 72 h (Zhan et al., 2009; Zhang et al., 2017; Zhang et al., 2019).

## 12 3 Results

### 13 3.1 Atmospheric CO<sub>2</sub> and CH<sub>4</sub> mixing ratios

14 Generally, CO<sub>2</sub> and CH<sub>4</sub> mixing ratios decreasing with increasing altitude and distance away  
15 from continent, and decreasing latitude (Matsueda et al., 1996; Bartlett et al., 2003; Zang et al.,  
16 2017). Spatiotemporal distributions of atmospheric CO<sub>2</sub> and CH<sub>4</sub> mixing ratios in shelf seas  
17 suggested not only natural characteristics, but also multiple anthropogenic processes, such as  
18 marine oil and gas exploration (Nara et al., 2014; Zang et al., 2020), land-sea air mass  
19 transportation (Kong et al., 2010; Liu et al., 2018), and malfunction of observation instrument  
20 (Zang et al., 2017).

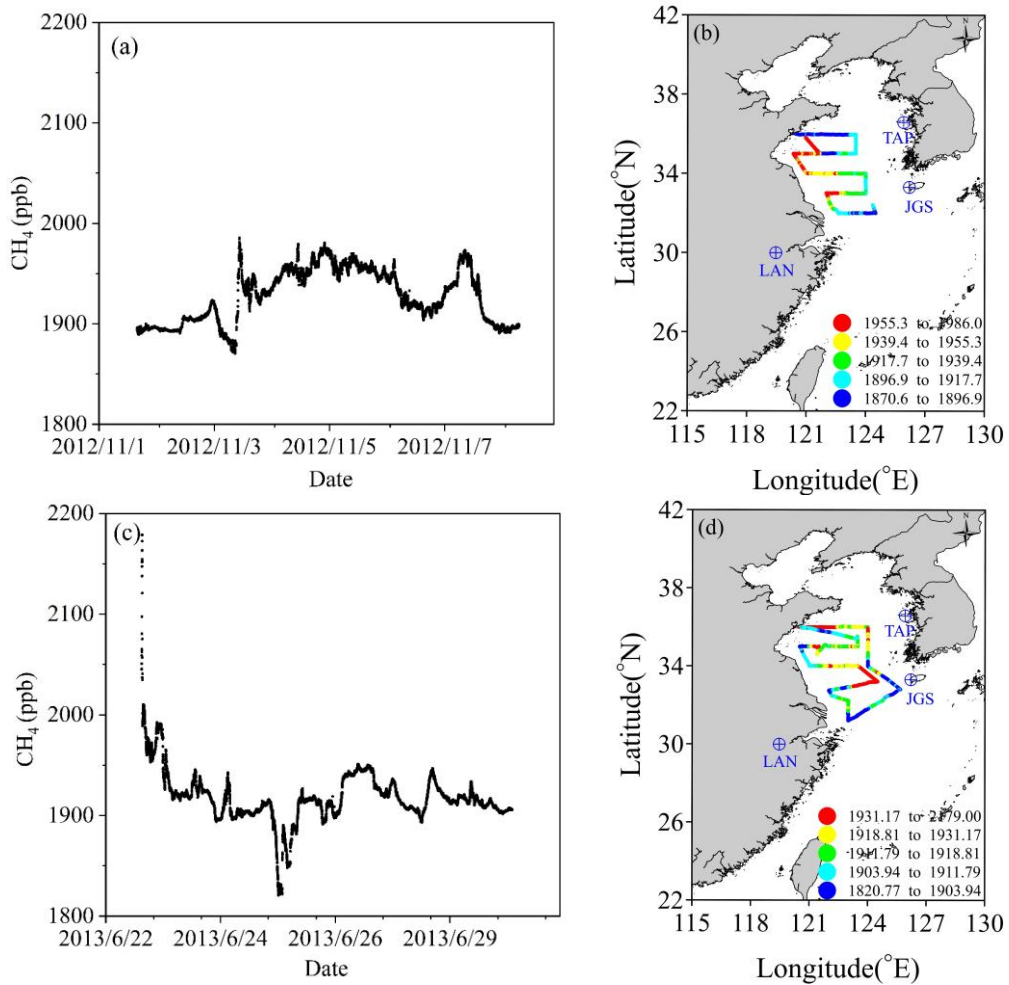


1

2 Fig. 3. Temporal (a and c) and spatial (b and d) distribution of CO<sub>2</sub> mixing ratios in

3 November 2012 and June 2013 in the SYS.





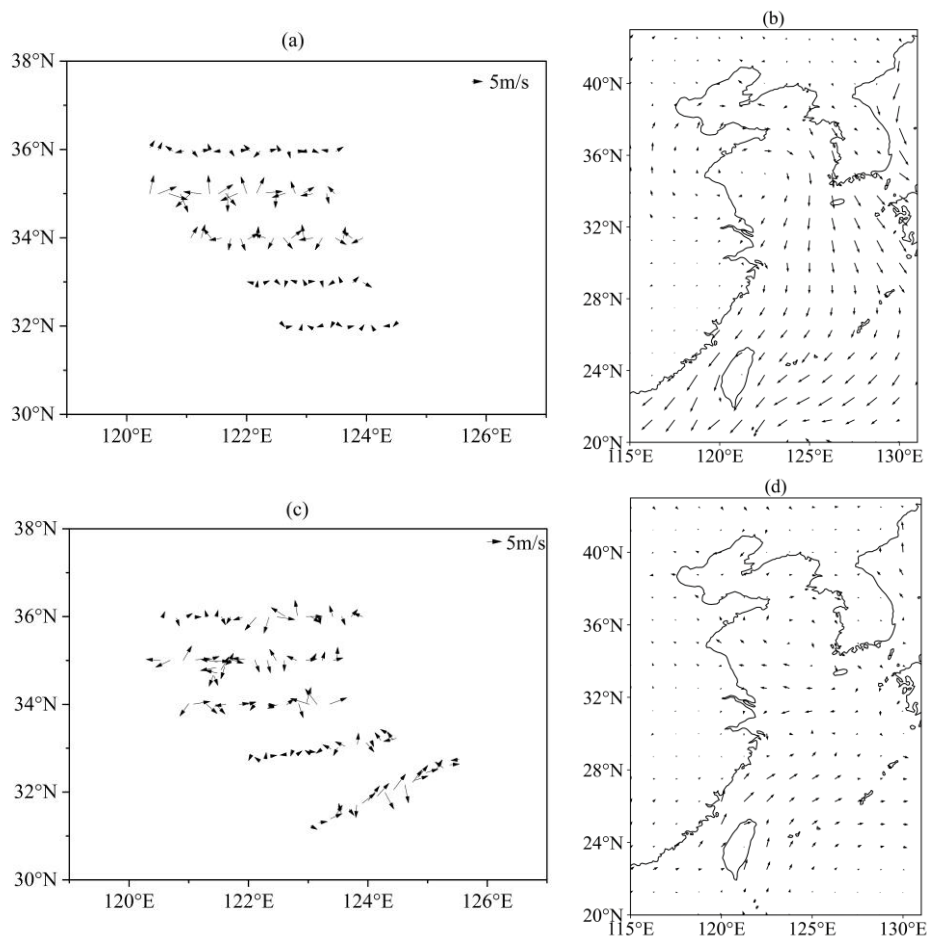
1  
2 Fig. 4. Temporal (a and c) and spatial (b and d) distribution of CH<sub>4</sub> mixing ratios in November and  
3 June of the SYS.

4 During the two field surveys, atmospheric CO<sub>2</sub> mixing ratios ranged from 392.75 ppm to  
5 688.10 ppm in November 2012 (Fig. 3a and Fig. 3b), and ranged from 389.28 ppm to 967.60 ppm  
6 in June 2013 (Fig. 3c and Fig. 3d), respectively. Atmospheric CH<sub>4</sub> mixing ratios ranged from  
7 1870.6 ppb to 1986.0 ppb in November 2012 (Fig. 4a and Fig. 4b), and ranged from 1820.8 ppb to  
8 2179.0 ppb in June 2013 (Fig. 4c and Fig. 4d), respectively. Atmospheric CO<sub>2</sub> and CH<sub>4</sub> mixing  
9 ratios were comparable with the historical observation results of the north hemisphere (Matsueda  
10 et al., 1996; Zang et al., 2017; Liu et al., 2018). Abnormal high observation values were  
11 attributed to exhaust gases of ship or anthropogenic interference of analyzer.

### 12 3.2 Wind data

13 Observed wind data were averaged to hourly data for subsequently analysis. As shown in  
14 Fig. 5a, during the survey of November 2012, hourly mean wind speed ranged from 0.05 to 20.46

1 m/s with an average value of 8.09 (4.17) m/s. Dominate wind direction was from north and  
2 northeast, indicated the air masses flowed from the Asia continent to the Pacific Ocean. As shown  
3 in Fig. 5c, during the survey of June 2013, hourly mean wind speed ranged from 0.08 m/s to 9.42  
4 m/s with an average value of 4.72 (1.79) m/s. Conversely, the predominant wind direction turned  
5 into south or southeast, which promoted air masses flowing from the Pacific Ocean to the Asia  
6 continent. In addition, the observed dominant wind directions (Fig. 5a and Fig. 5c) were consisting  
7 well with the simulated wind fields (Fig. 5b and Fig. 5d), suggested the typical features of winter  
8 and summer monsoon, which were ideal cases to study effects of land-sea air masses  
9 transportation on the spatiotemporal variations of CO<sub>2</sub> and CH<sub>4</sub> mixing ratios in the MBL of the  
10 SYS.



11  
12 Fig. 5. Observed wind direction and speed (a and c) and simulation of wind fields (b and d)  
13 over the SYS. The simulated wind fields were plotted based on the ERA5 hourly data on pressure  
14 levels provided by the European Centre for Medium-Range Weather Forecasts (ECMWF),  
15 (<https://cds.climate.copernicus.eu/cdsapp#!/dataset/reanalysis-era5-pressure-levels?tab=form>,  
16 download date: 2022-11-04).

1 4. Discussion

2 4.1 Data filter approach

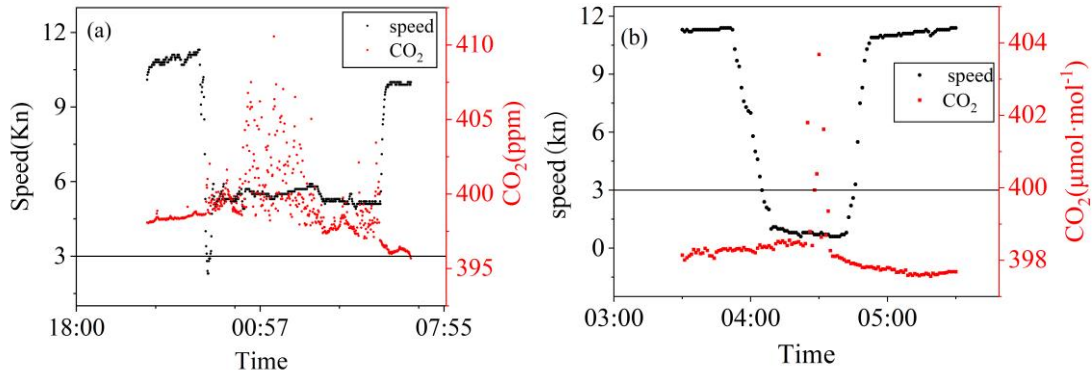
3 Although some empirically based data processes have been reported (Zang et al., 2017; Liu et  
4 al., 2018), a specific data filtering approach for shipborne continuous observation need to be  
5 optimized and established to distinguish impacts of multiple source-sink processes on shipborne  
6 observed atmospheric CO<sub>2</sub> and CH<sub>4</sub> mixing ratios along the cruise tracks, especially in the shelf  
7 seas.

8 Firstly, observed atmospheric CO<sub>2</sub> and CH<sub>4</sub> mixing ratios along the cruise tracks in  
9 November 2012 and June 2013 were calibrated by a linear function, averaged every one minute,  
10 and named as Raw Data for the subsequently process.

11 Secondly, according to voyage record, the abnormal values that caused by mal-function of  
12 instrument and impacted by manually refilling the drying-tube were flagged (Zang et al., 2017).

13 Thirdly, when the ship stopping for oceanography investigating at discrete stations or  
14 cruising downwind with speed lower than wind speed, observed atmospheric CO<sub>2</sub> and CH<sub>4</sub> mixing  
15 ratios might be impacted by ship's exhaust gas and human activities (Zang et al., 2017; Liu et al.,  
16 2018). Previous studies considered 3 knots as the criterion to flag data influenced by ship's  
17 exhaust gas and human activities by observation experience (Zang et al., 2017; Liu et al., 2018).

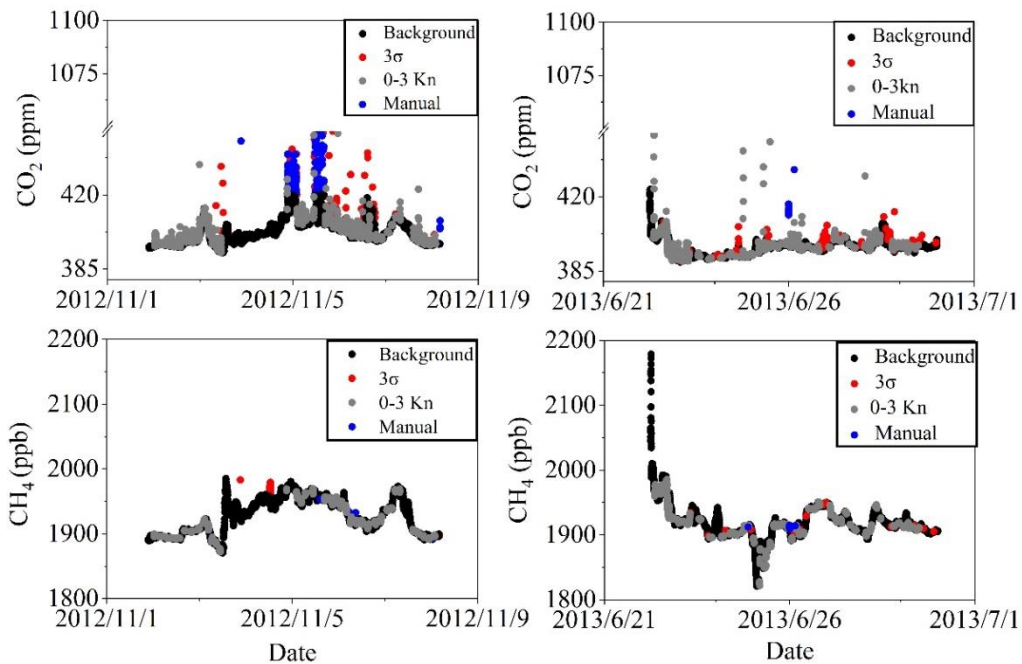
18 In this study, take two station measurement as examples, as showed in Fig. 6a and Fig. 6b,  
19 when ship speed slowed down from normal cruising speed of 11 knots to less than 3 knots, the  
20 observed CO<sub>2</sub> mixing ratio varied from a smooth pattern with SD (standard deviation) value less  
21 than 0.10 ppm to intensive fluctuation pattern with SD value greater than 1.20 ppm, due to  
22 influences of ship emissions and human activities. According to the quality control criteria of CO<sub>2</sub>  
23 ( $\pm 0.10$  ppm), which recommended by the World Meteorological Organization Global  
24 Atmospheric Watch (WMO/GAW) (WMO 2005), 3 knots was optimized as the threshold. Results  
25 showed that, 15.5% and 21.9% of total observed data in November 2012 and June 2013,  
26 respectively, were flagged in this step.



1

2 Fig. 6. Variations of observed CO<sub>2</sub> mixing ratios and ship speed from 20:40 on 28<sup>th</sup> to 6:40 on 29<sup>th</sup>  
 3 June 2013 (a) and 3:30 to 5:30 on 3<sup>th</sup> November 2012(b).

4 Finally, the Pauta criterion (“3σ” method), a widely used data quality control approach in  
 5 atmospheric greenhouse gas observation (Zhang et al., 2007; Zhang et al., 2013; Fang et al., 2015;  
 6 Zang et al., 2017), was introduced to filter and flag the non-background measurement results. To  
 7 optimize this process, observation data that covered period of 0.5, 1, 2 and 4 hour was calculated,  
 8 respectively. Any deviation between observed results and average value lying outside ± 3 SD was  
 9 considered as non-background data and should be flagged. This procedure was repeated until no  
 10 outliers were identified (Zhang et al., 2007). Result showed that data calculated hourly was  
 11 optimal, because it could not only flag dispersed values, but keep the smooth data well.



12

13 Fig. 7. Filtered results of CO<sub>2</sub> (a, b) and CH<sub>4</sub> (c, d) mixing ratios in November 2012 and June

1 2013, the ordinates of a and b are broken in the range of 450 to 1050 ppm. Black points represent  
2 the background data (Background). Blue points represent data influenced by replacing dry tube  
3 that were manually flagged (Manual). Green points mean the data influenced by ship emissions at  
4 low speed (less than 3 knots). Red points represent the data filtered out by the Pauta criterion ( $3\sigma$ ).

5 As shown in Fig. 7, based on the optimized approach, observed data could be filtered and  
6 flagged. The remained data accounted for 79.5% and 75.7% of raw data in November 2012 and  
7 June 2013, respectively, which were considered as background represents, and used for further  
8 analysis.

9 Observed mean CO<sub>2</sub> mixing ratios were 403.94 (13.77) ppm and 395.90 (3.53) ppm in  
10 November 2012 and June 2013, respectively, which were slightly lower than previous studies'  
11 mean values of 405 ppm and 410 ppm in the YS and ECS in March 2013 and March 2017,  
12 respectively (Zang et al., 2017; Liu et al., 2018). Moreover, observed mean atmospheric CO<sub>2</sub>  
13 mixing ratio was almost equal to results observed at the TAP (401.37 ppm) and JGS (403.77 ppm)  
14 stations, but approximate 9 ppm higher than MBL-CO<sub>2</sub> reference (394.41 to 394.78 ppm in  
15 latitude zone of 30 °N to 37 °N) (<https://gml.noaa.gov/ccgg/mbl/data.php> download data: 2022-  
16 10-10) in November 2012, and almost equal to results observed at the LAN (396.43 ppm) and JGS  
17 (398.10 ppm) stations and MBL-CO<sub>2</sub> reference (397.38 to 397.92 ppm in latitude zone of 30 °N to  
18 37 °N) in June 2013.

19 Observed mean CH<sub>4</sub> mixing ratios were 1924.8 (27.8) ppb and 1918.0 (25.7) ppb in  
20 November 2012 and June 2013, respectively, which were slightly higher than historical data of  
21 1915.5 ppb in the SYS in March 2013 (Zang et al., 2017), and higher than the MBL-CH<sub>4</sub>  
22 references of November 2012 (1869.5 to 1880.3 ppb) and June 2013 (1835.3 to 1846.6 ppb).

#### 23 4.2 Influence of air-sea exchange on distribution of atmospheric CO<sub>2</sub> and CH<sub>4</sub> mixing ratios

24 Air-sea exchange is a dynamic process when CO<sub>2</sub> and CH<sub>4</sub> molecules diffusing via the  
25 interface of surface seawater and overlying atmosphere. Source and sink of atmospheric CO<sub>2</sub> and  
26 CH<sub>4</sub> mean they were emitted from or absorbed by seawater. In fact, the magnitude of air-sea CO<sub>2</sub>  
27 and CH<sub>4</sub> exchange varied dramatically in spatial and temporal scale in coastal shallow seas (Yang  
28 et al., 2016; Gao et al., 2019). Generally, CO<sub>2</sub> and CH<sub>4</sub> emitted from the seawater into the air were  
29 difficult to trace by atmospheric measurements because they could dilute sharply (Schmale et al.,

1 2005; Kourtidis et al., 2006; Zhai et al., 2013), only shallow seeps areas and coastal regions, could  
2 influence mixing ratios of local atmospheric CO<sub>2</sub> and CH<sub>4</sub> directly and be measured (Leifer et al.,  
3 2006; Luo et al., 2015). Despite the dissolved CO<sub>2</sub> and CH<sub>4</sub> were not observed in our field  
4 surveys, the published data showed that sea-to-air CO<sub>2</sub> fluxes were 6.0 (8.8 mmol/m<sup>2</sup>/day in  
5 November 2012 and 2.6 (4.3) mmol/m<sup>2</sup>/day in June 2011 (Wang and Zhai, 2021), and sea-to-air  
6 CH<sub>4</sub> fluxes were 6.4 μmol/m<sup>2</sup>/day in November 2002 and 15.7 μmol/m<sup>2</sup>/day in June 2006 (Zhang  
7 et al., 2008), respectively, in the SYS.

8 To estimate the effects of air-sea exchange on mixing ratios of atmospheric CO<sub>2</sub> and CH<sub>4</sub>, we  
9 used a simple method described by Kourtidis et al. (2006) and optimized by Zang et al. (2020):  
10 assumed that a box located above the survey area, with a ceiling of 10 meters which  
11 corresponding to the height of air inlet in our field surveys. The contents of atmospheric CO<sub>2</sub> and  
12 CH<sub>4</sub> were only impacted by air-sea exchange. When CO<sub>2</sub> and CH<sub>4</sub> were vented into or absorbed  
13 from the box, their mixing ratios would increase or decrease homogeneously, caused by the mean  
14 calculated results of sea-to-air CO<sub>2</sub> and CH<sub>4</sub> fluxes.

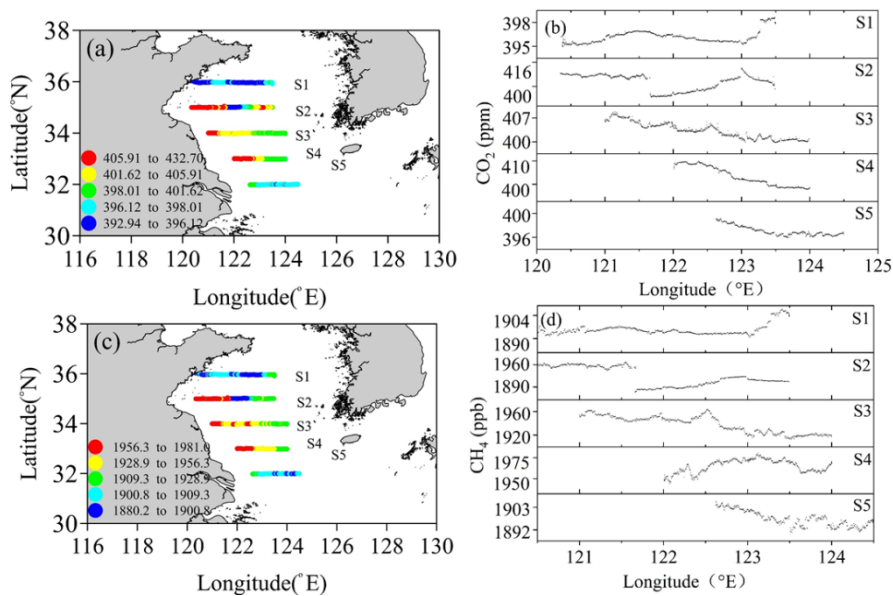
15 Generally, coastal shallow seas are source of atmospheric CH<sub>4</sub>, accounting for approximate  
16 75% of global ocean emissions (Bange et al., 1994; Bates et al., 1996). However, according to the  
17 calculation formula that given by Zang et al. (2020), sea-to-air CH<sub>4</sub> flux of 50.8 μmol/m<sup>2</sup>/day  
18 could result in an increasing of 2 ppb of atmospheric CH<sub>4</sub> mixing ratio in the MBL. Thus, the  
19 impacts of the reported mean sea-to-air CH<sub>4</sub> fluxes (6.4 μmol/m<sup>2</sup>/day and 15.7 μmol/m<sup>2</sup>/day in  
20 November 2002 and June 2006) on the atmospheric CH<sub>4</sub> would not exceed 1 ppb (Zhang et al.,  
21 2008). In addition, based on the same method, the impacts of the reported mean sea-to-air CO<sub>2</sub>  
22 fluxes (Wang and Zhai, 2021) on the atmospheric CO<sub>2</sub> mixing ratios were calculated, which was  
23 no more than 14.1 ppb. Thus, it was reasonable to conclude that influences of air-sea exchange on  
24 distribution of atmospheric CO<sub>2</sub> and CH<sub>4</sub> mixing ratios were slight or negligible, compared to the  
25 observed variability of atmospheric CO<sub>2</sub> and CH<sub>4</sub> (Fig.3 and Fig. 4).

#### 26 4.3 Influences of land–sea air mass transportation on spatiotemporal distribution of atmospheric 27 CO<sub>2</sub> and CH<sub>4</sub> mixing ratios

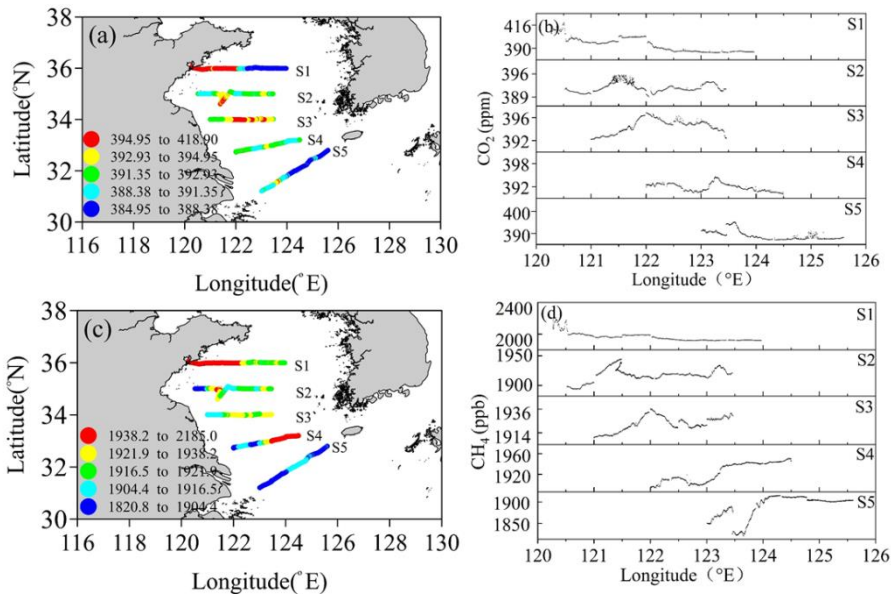
28 The EAWM is closely related to atmospheric compounds transportation from the Asia  
29 Continent to the Western Pacific (Yu et al., 2014). Since two surveys were conducted in

1 November 2012 and June 2013, when the typical winter and summer monsoon season in their  
 2 early phases, respectively (Lyu et al., 2021; Lin'an et al., 2022), the observation data could give us  
 3 an ideal opportunity to study the impacts of land-to-sea air mass transportation on spatiotemporal  
 4 distribution of atmospheric CO<sub>2</sub> and CH<sub>4</sub> mixing ratios over the SYS. Observed atmospheric CO<sub>2</sub>  
 5 and CH<sub>4</sub> mixing ratios were higher in November 2012 (Fig. 8) than that in July 2013 (Fig. 9).  
 6 Except for the Section 1 (S1) and the right end of Section 2 (S2), the spatial distributions were  
 7 gradient descent with offshore distance (Fig. 8).

8 In situ observed data demonstrated that the dominant wind direction was W-NW-NNW for  
 9 section 2, 3, 4 and 5 in November 2012, suggested the air masses were transported from the Asian  
 10 Continent to the Pacific Ocean (Fig. 5 and Supplementary data). Generally, CO<sub>2</sub> and CH<sub>4</sub> mixing  
 11 ratios were higher in continent than that of the MBL (Zhang et al., 2007; Zang et al., 2017; Liu et  
 12 al., 2018), land-to-sea air mass transportation driven by the EAWM could result in the horizontal  
 13 transmission of greenhouse gases. Due to the subsequently mixing and dilution, CO<sub>2</sub> and CH<sub>4</sub>  
 14 mixing ratios would decline along the windward (Bartlett et al., 2003; Kourtidis et al., 2006; Liu et  
 15 al., 2018). Meanwhile, the mixing ratios of atmosphere CO<sub>2</sub> and CH<sub>4</sub> were low and homogeneous  
 16 in Section 1 and right end of Section 2, because the dominant wind direction was ENE-SE-S,  
 17 indicated air masses were transported from the open Pacific Ocean with low content of CO<sub>2</sub> and  
 18 CH<sub>4</sub> (Matsuda, 1996; Bartlett et al., 2003; Zang et al., 2017).



19  
 20 Fig. 8. Spatial distributions of CO<sub>2</sub> and CH<sub>4</sub> mixing ratios in the survey area in November

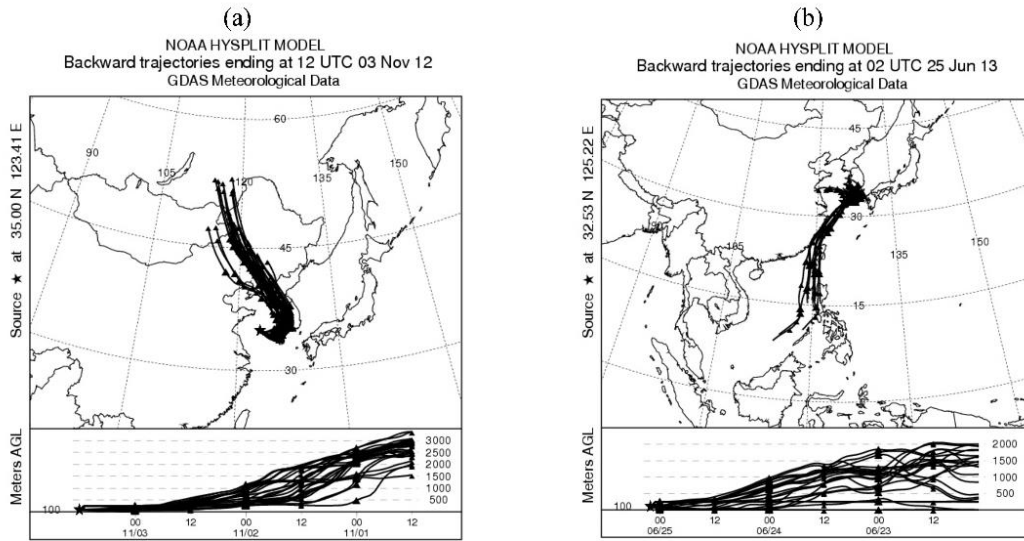


2

3 Fig. 9. Spatial distributions of CO<sub>2</sub> and CH<sub>4</sub> mixing ratios in the survey area in July 2013.

4 Furthermore, back trajectory analysis showed that almost all the transport tracks were  
 5 originated from the Asian Continent in November 2012, and the South China Sea and West  
 6 Pacific Ocean in July 2013 (typical characteristics of the early summer monsoon) (Fig. 10), which  
 7 resulted in higher atmospheric CO<sub>2</sub> and CH<sub>4</sub> mixing ratios in November 2012 (Fig. 8) than that in  
 8 July 2013 (Fig. 9). Seasonal variations of atmospheric CO<sub>2</sub> and CH<sub>4</sub> mixing ratios were consistent  
 9 with the variations of atmospheric CO<sub>2</sub> mixing ratios in West Pacific Ocean, where atmospheric  
 10 components distributions were dominated by maritime air masses from the Pacific Ocean and  
 11 polluted air masses from the Asian Continent (Matsuda, 1996; Zhang et al., 2007; Liu et al., 2018).

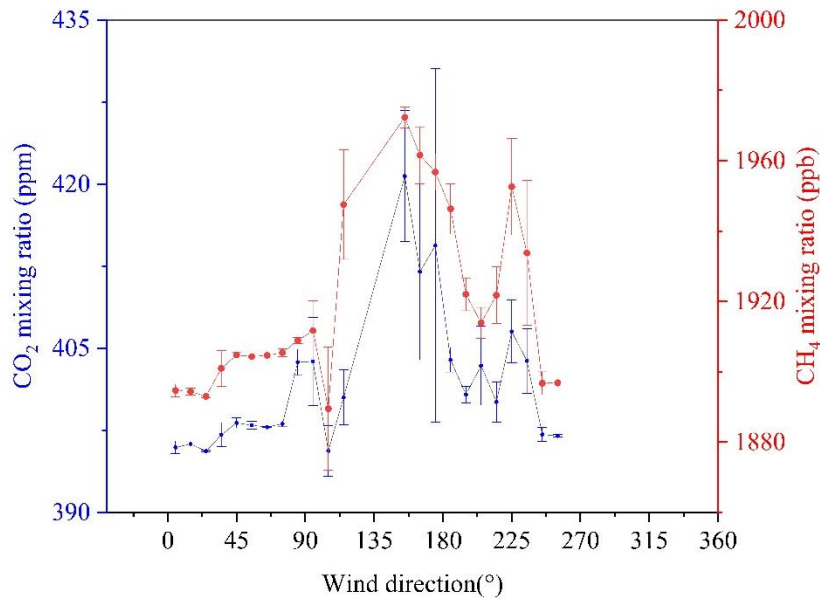




1  
2 Fig. 10. Three-day air back-trajectories of two typical locations, a (35.00 °N, 123.41 °E) and b  
3 (32.53 °N, 125.22 °E).

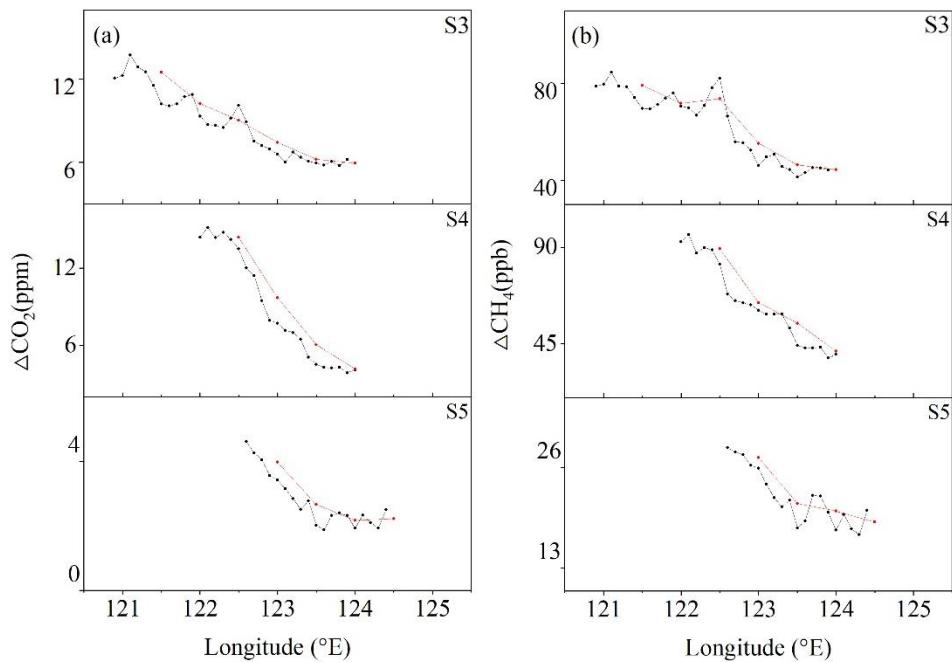
4 4.4 Estimated distance of land-to-sea air mass transportation

5 As shown in Fig. 11, atmospheric CO<sub>2</sub> and CH<sub>4</sub> mixing ratios observed in November 2012  
6 showed the same fluctuating feature versus wind direction, indicated their variations were  
7 dominated by the land-to-sea air masses transportation, which was in agreement with previous  
8 studies (Zhang et al., 2007; Zang et al., 2017; 2020; Liu et al., 2018).



9  
10 Fig. 11. Relationship between wind direction and atmospheric mixing ratios of CO<sub>2</sub> and CH<sub>4</sub>,  
11 respectively. Error bars indicated standard deviations in each wind direction.

1 Simulation studies of gas seeps in the Black Sea and the Nord Stream pipeline gas leaks in  
 2 the Baltic Sea showed that atmospheric CH<sub>4</sub> mixing ratio could be enhanced by the upwind  
 3 emission source in distance of 5 to 30 km (Kourtidis et al., 2006; Jia et al., 2022). NOAA's MBL-  
 4 CO<sub>2</sub> and MBL-CH<sub>4</sub> references were 394.56 ppm and 1875.4 ppb, respectively, at the same latitude  
 5 zone with the survey area in November 2012.  $\Delta\text{CO}_2$  and  $\Delta\text{CH}_4$  represented deviations between  
 6 observed atmospheric CO<sub>2</sub> and CH<sub>4</sub> mixing ratios and MBL-CO<sub>2</sub> and MBL-CH<sub>4</sub> references. As  
 7 shown in Fig. 12, we assumed that the effects of mixing and dilution during the transportation was  
 8 linear (Kourtidis et al., 2006), the further the observation site away from continent, the lower the  
 9  $\Delta\text{CO}_2$  and  $\Delta\text{CH}_4$  values in each survey section. According to the calculated slope values, gradient  
 10 would be gradual at 123.30 °E, 123.50 °E and 123.40 °E for section 3, 4 and 5, respectively.  
 11 Moreover, the offshore distances away from continent could be calculated as approximate 27.0,  
 12 26.3 and 11.7 km, respectively, with a mean value of 21.7 km. Thus, spatial distributions of  
 13 atmospheric CO<sub>2</sub> and CH<sub>4</sub> mixing ratios in the China shelf sea could be impacted remarkably by  
 14 land-to-sea air mass transportation during early phase of the EAWM.



15  
 16 Fig. 12. The average value of  $\Delta\text{CO}_2$  (a) and  $\Delta\text{CH}_4$  (b) per 0.1 (black) or 0.5 longitude (red) in  
 17 November 2012.

18 5. Conclusions

19 Based on the shipborne continuously observed atmospheric CO<sub>2</sub> and CH<sub>4</sub> mixing ratios and

1 meteorological parameters over the SYS in November 2012 and June 2013, a data filter method  
2 was optimized and established, which could be used to flag CO<sub>2</sub> and CH<sub>4</sub> mixing ratios influenced  
3 by multiple natural processes and human activities. Spatial and seasonal variations of atmospheric  
4 CO<sub>2</sub> and CH<sub>4</sub> mixing ratios over the SYS were mainly regulated by the EAM, while the influence  
5 of air-sea exchange was slight or negligible. Summer monsoon resulted in relatively low  
6 atmospheric CO<sub>2</sub> and CH<sub>4</sub> mixing ratios with a gradient increasing from southeast to northwest.  
7 Conversely, winter monsoon enhanced land-to-sea air masses transportation with high  
8 atmospheric CO<sub>2</sub> and CH<sub>4</sub> mixing ratios, which induced decreasing patterns with increasing  
9 distance offshore. Effect of land-to-sea air mass transportation on enhanced CO<sub>2</sub> and CH<sub>4</sub> mixing  
10 ratios was quantification with a distance of approximate 20 km offshore during the early period of  
11 the EAWM.

12  
13 *Code availability.* The code that is used for figure plotting (python) can be provided upon  
14 request.

15 *Data availability.* The ERA5 hourly data on pressure levels provided by the European Centre  
16 for Medium-Range Weather Forecasts (ECMWF),  
17 <https://cds.climate.copernicus.eu/cdsapp#!/dataset/reanalysis-era5-pressure-levels?tab=form>,  
18 download date: 2022-11-04). The simulated MBL values produced by NOAA,  
19 [www.esrl.noaa.gov/gmd/ccgg/GHGreference](http://www.esrl.noaa.gov/gmd/ccgg/GHGreference), download data: 2022-10-10.

## 20 **Author contributions**

21 Jiaxin Li prepared the main part of the paper and performed the corresponding analyses.  
22 Kunpeng Zang provided the original data that are used within this study and helped with the data  
23 analyses and the preparation of the paper. Yi Lin, Yuanyuan Chen, Shuo Liu, Honghui Xu and  
24 Yujun Jiang provided valuable comments on data processing and, as well as help in the drawing of  
25 Fig. 5. Shuangxi Fang, Shanshan Qiu and kai Jiang suggestions for revising the paper and further  
26 standardized the paper. Haoyu Xiong, Xuemei Qing and Haixiang Hong helped download the  
27 MBL-references data.

## 28 **Competing interest**

29 This manuscript is approved by all authors for publication, and we have no competing interests

1 to declare that are relevant to the content of this article.

## 2 **Acknowledgments**

3 The authors wish to thank the crew of the R/V “Dongfanghong II” for their assistance on  
4 board. We also thank Dr. E. J. Dlugokencky and colleagues from the Tae-ahn Peninsula station,  
5 Jeju Gosan station and Lin’an station. This work was supported by the National Key Research and  
6 Development Program of China (2020YFA0607501), the National Natural Science Foundation of  
7 China (No. 42275113), the Special Support Plan for High-level Talents in Zhejiang province  
8 (2021R542048), the Joint funds of the Zhejiang Provincial Natural Science Foundation of China  
9 under Grant No. LZJMZ23D050002, the Fund of Key Laboratory of Global Change and Marine-  
10 Atmospheric Chemistry, MNR (GCMAC2001) and the Basic Public Welfare Research Program of  
11 Zhejiang Province (LGF22D050004).

1 **References**

2 AGGI. The NOAA annual greenhouse gas index (AGGI). NOAA Earth System Research Laboratory,  
3 Boulder, Colorado, USA. <http://esrl.noaa.gov/gmd/aggi/aggi.html>, 2014.

4 Bange, H. W., Bartell, U. H., Rapsomanikis, S., and Andre, M. O.: Methane in the Baltic and North Seas and  
5 a Reassessment of the Marine Emissions of Methane, *Global Biogeochem Cy.*, 8, 465-480,  
6 <https://doi.org/10.1016/j.marchem.2008.02.005>, 1994.

7 Bartlett, K. B., Sachse, G. W., Slate, T., Harward, C., and Blake, D. R.: Large-scale distribution of CH<sub>4</sub> in the  
8 western North Pacific: Sources and transport from the Asian continent, *J. Geophys. Res-Atmos.*, 108, D20,  
9 <https://doi:10.1029/2002JD003076>, 2003.

10 Bouman, E. A., Lindstad, E., Rialland, A. I., and Stomman, A. H.: State-of-the-art technologies, measures,  
11 and potential for reducing GHG emissions from shipping-A review, *Transport. Res. D-Tr. E*, 52, 408-421,  
12 <http://dx.doi.org/10.1016/j.trd.2017.03.022>, 2017.

13 Chang, C., L. Yi, and Chen, G. T.: A numerical simulation of vortex development during the 1992 east Asian  
14 summer monsoon onset using the navy's regional model, *Mon. Wea. Rev.*, 128, 1604–1631,  
15 [https://doi.org/10.1175/1520-0493\(2000\)128<1604:ANSOVD>2.0.CO;2](https://doi.org/10.1175/1520-0493(2000)128<1604:ANSOVD>2.0.CO;2), 2000.

16 Crosson, E. R.: A cavity ring-down analyzer for measuring atmospheric levels of methane, carbon dioxide,  
17 and water vapor, *App. Phys. B-Lasers. O.*, 92, 403-408, <https://10.1007/s00340-008-3135-y>, 2008.

18 Dlugokencky, E. J., Myers, R. C., Lang, P. M., Masarie, K. A., Crotwell, A. M., Thoning, K. W., Hall, B. D.,  
19 Elkins, J. W., and Steele, L. P.: Conversion of NOAA atmospheric dry air CH<sub>4</sub> mole fractions to a gravimetrically  
20 prepared standard scale, *J. Geophys. Res.*, 110, D18306, <https://doi.org/10.1029/2005JD006035>, 2005.

21 Ding, Y. H., Liu, J. J., Sun, Y., Liu, Y., He, J., and Song, Y.: A study of the synoptic-climatology of the  
22 Meiyu system in East Asia, *Chinese Journal of Atmospheric Sciences*, 31, 1082-1101, 2007.

23 Ding, J., Van Der A, R. J., Mijling, B., Jalkanen, J. P., Johansson, L., and Levelt, P. F.: Maritime NOx  
24 emissions over Chinese Seas derived from satellite observations, *Geophys. Res. Lett.*, 45, 2031-2037,  
25 <https://doi.org/10.1002/2017GL076788>, 2018.

26 Fang, S. X., Zhou, L. X., Masarie, K. A., Xu, L., and Rella, C. W.: Study of atmospheric CH<sub>4</sub> mole fractions  
27 at three WMO/GAW stations in China, *J. Geophys. Res-Atmos.*, 118, 4874-4886,  
28 <https://doi.org/10.1002/jgrd.50284>, 2013.

29 Fang, S. X., Tans, P. P., Steinbacher, M., Zhou, L. X., and Luan, T.: Comparison of the regional CO<sub>2</sub> mole

1 fraction filtering approaches at a WMO/GAW regional station in China, *Atmos. Meas. Tech.*, 8, 5301-5313,  
2 <https://doi.org/10.5194/amt-8-5301-2015>, 2015.

3 Gao, Z. M., Liu, H. P., and Mcfarland, D. P.: Mechanistic links between underestimated CO<sub>2</sub> fluxes and non-  
4 closure of the surface energy balance in a semi-arid sagebrush ecosystem, *Enviro. Res. Lett.*, 14, 1748-9326,  
5 <https://doi.org/10.1088/1748-9326/ab82d>, 2019.

6 Huang, R. H.: The influence of the heat source anomaly over Tibetan Plateau on the northern hemispheric  
7 circulation anomalies, *Acta. Meteorol. Sin.*, 43, 208-220, 1985.

8 Houghton, R. H., Zhou, L. T., and Chen, W.: The progresses of recent studies on the variabilities of the East  
9 Asian monsoon and their causes, *Adv. Atmos. Sci.*, 20, 55-69, 2003.

10 Jia, M., Li, F., Zhang, Y. Z., Wu, M. S., Li, Y. S., Feng, S. Z., Wang, H. M., Chen, H. L., Ju, W. M., Lin, J.,  
11 Cai, J. W., Zhang, Y. G., and Jiang, F.: The Nord Stream pipeline gas leaks released approximately 220,000 tonnes  
12 of methane into the atmosphere, *Environmental Science and Ecotechnology*, 12, 2666-4984, [https://](https://doi.org/10.1016/j.es.2022.100210)  
13 [doi.org/10.1016/j.es.2022.100210](https://doi.org/10.1016/j.es.2022.100210), 2022.

14 Kourtidis, K., Kioutsioukis, I., McGinnis, D. F., and Rapsomanikis, S.: Effects of methane outgassing on the  
15 Black Sea atmosphere, *Atmos. Chem. Phys.*, 6, 5173–5182, <https://doi.org/10.5194/acp-6-5173-2006>, 2006.

16 Kong, S., Lu, B., Han, B., Bai, Z. P., Xu, Z., You, Y., Jin, L. M., Guo, X. Y., and Wang, R.: Seasonal  
17 variation analysis of atmospheric CH<sub>4</sub>, N<sub>2</sub>O and CO<sub>2</sub> in Tianjin offshore area. *Sci. China Earth Sci.*, 53, 1205–  
18 1215, <https://doi.org/10.1007/s11430-010-3065-5>, 2010.

19 Law, C. S., Brévière, E., De Leeuw, G., Garçon, V., Guieu, C., Kieber, D. J., Konradowitz, S., Paulmier, A.,  
20 Quinn, P. K., Saltzman, E. S., Stefels, J., and Von Glasow, R.: Evolving research directions in Surface Ocean-  
21 Lower Atmosphere (SOLAS) science, *Environ. Chem.*, 10, 1-16, <https://doi.org/10.1071/EN12159>, 2013.

22 Luo, X. F., Wei, H., Liu, Z., and Zhao, L.: Seasonal variability of air–sea CO<sub>2</sub> fluxes in the Yellow and East  
23 China Seas: A case study of continental shelf sea carbon cycle model, *Cont. Shelf. Res.*, 107, 69-78,  
24 <http://dx.doi.org/10.1016/j.csr.2015.07.009>, 2015.

25 Liu, Y. S., Zhou, L. X., Tans, P. P., Zang, K. P., and Cheng, S. Y.: Ratios of greenhouse gas emissions  
26 observed over the Yellow Sea and the East China Sea, *Sci. Total. Environ.*, 33, 1022-1031  
27 <https://doi.org/10.1016/j.scitotenv.2018.03.250>, 2018.

28 Lyu, W. Z., Fu, T. F., Hu, Z. X., Tang, Y. Z., Chen, G. Q., Xu, X. Y., Chen, Y. P., and Chen, S. L.: Sedimentary  
29 dynamics of the central South Yellow Sea revealing the relation between east Asian Summer and Winter Monsoon

1 over the past 6000 years, *Front. Earth Sci.*, 9, 689508, <https://doi.org/10.3389/feart.2021.689508>, 2021.

2 Masarie, K. A., and Tans, P. P.: Extension and integration of atmospheric carbon-dioxide data into a globally  
3 consistent measurement record. *J. Geophys. Res-Atmos.*, 100, 11593-11610, <https://doi.org/10.1029/95JD00859>,  
4 1995.

5 Matsueda, H., Inoue, H. Y., Ishii, M., and Nogi, Y.: Atmospheric methane over the North Pacific from 1987  
6 to 1993. *Geochem. J.*, 30, 1-15, 1996.

7 Nara, H., Tanimoto, H., Tohjima, Y., Mukai, H., Nojiri, Y., and Machida, T.: Emissions of methane from  
8 offshore oil and gas platforms in Southeast Asia, *Sci Rep* 4, 6503, <https://doi.org/10.1038/srep06503>, 2014.

9 Peters, G., Marland, G., Le Quéré, C., Boden, T., Canadell, J. G., and Raupach, M. R.: Rapid growth in CO<sub>2</sub>  
10 emissions after the 2008-2009 global financial crisis, *Nat. Clim. Change.*, 2, 2-4,  
11 <https://doi.org/10.1038/nclimate1332>, 2012.

12 Rella, C. W., Chen, H., Andrews, A. E., Filges, A., Gerbig, C., Hatakka, J., Karion, A., Miles, N. L.,  
13 Richardson, S. J., Steinbacher, M., Sweeney, C., Wastine, B., and Zellweger, C.: High accuracy measurements of  
14 dry mole fractions of carbon dioxide and methane in humid air, *Atmos. Meas. Tech.*, 6, 837-860,  
15 <https://doi.org/10.5194/amt-6-837-2013>, 2013.

16 Riddick, S. N., Mauzerall, D. L., Cella, M., Harris, N. R. P., Allen, G., Pitt, J., Staunton-Sykes, J., Forster, G.  
17 L., Kang, M., Lowry, D., Nisbet, E. G., and Manning, A. J.: Methane emission from oil and gas platforms in the  
18 North Sea. *Atmos. Chem. Phys.*, 19, 9787-9796, <https://doi.org/10.5194/acp-19-9787-2019>, 2019.

19 Schmale, O., Greinert, J., and Rehder, G.: Methane emission from high-intensity marine gas seeps in the  
20 Black Sea into the atmosphere, *Geophys. Res. Lett.*, 32, 7, <https://doi.org/10.1029/2004GL021138>, 2005.

21 Warneke, T., De Beek, R., Buchwitz, M., Notholt, J., Schulz, A., Velasco, V., and Schrems, O.: Shipborne  
22 solar absorption measurements of CO<sub>2</sub>, CH<sub>4</sub>, N<sub>2</sub>O and CO and comparison with SCIAMACHY WFM-DOAS  
23 retrievals, *Atmos. Chem. Phys.*, 5, 2029-2034, <https://doi.org/10.5194/acp-5-2029-2005>, 2005.

24 WMO, 12<sup>th</sup> WMO/IAEA Meeting of experts on carbon dioxide concentration and related tracers  
25 measurement techniques. NO. 161[R]. Toronto, Canada, 2005.

26 Wang, S. Y., and Zhai, W. D.: Regional differences in seasonal variation of air-sea CO<sub>2</sub> exchange in the  
27 Yellow Sea. *Cont. Shelf. Res.*, 218, 104393, <https://doi.org/10.1016/j.csr.2021.104393>, 2021.

28 WMO. Greenhouse Gas Bulletin: The state of greenhouse gases in the atmosphere based on global  
29 observations through 2021. <http://www.wmo.int/pages/prog/arep/gaw/ghg/ghgbull06en.html>, 2022.

1 Xia, L. J., Liu, L. X., Li, B. Z., and Zhou, L. X.: Spatial and temporal distribution characteristics of  
2 atmospheric CO<sub>2</sub> in central China, *China Environmental Science*, 38, 2811-2819,  
3 <https://doi.org/10.19674/j.cnki.issn1000-6923.2018.0294>, 2018.

4 Yu, G., Chen, Z., Piao, S. L., Peng, C. H., Ciais, P., Wang, Q. F., Li, X. R., and Zhu, X. J.: High carbon  
5 dioxide uptake by subtropical forest ecosystems in the East Asian monsoon region. *Proc. Natl. Acade. Sci. U. S.*,  
6 111, 4910-4915, <https://doi.org/10.1073/pnas.1317065111>, 2014.

7 Yang, M., Bell, T. G., Hopkins, F. E., Kitidis, V., Cazenave, P. W., Nightingale, P. D., Yelland, M. J., Pascal,  
8 R. W., Prytherch, J., Brooks, I. M., and Smyth, T. J.: Air-sea fluxes of CO<sub>2</sub> and CH<sub>4</sub> from the Penlee Point  
9 Atmospheric Observatory on the south-west coast of the UK, *Atmos. Chem. Phys.*, 16, 5745-5761,  
10 <https://doi.org/10.5194/acp-16-5745-2016>, 2016.

11 Zhan, L. Y., and Chen, L. Q.: Distribution characteristics of atmospheric nitrous oxide in the Southern  
12 Ocean, *Chinese Journal of Polar Research*, 2007, 49-60, 2007.

13 Zhan, R. F., and Li, J. P.: Influence of atmospheric heat sources over the Tibetan Plateau and the tropical  
14 western North Pacific on the inter-decadal variations of the stratosphere-troposphere exchange of water vapor, *Sci.*  
15 *China Ser. D-Earth Sci.*, 51, 1179-1193, <https://doi.org/10.1007/s11430-008-0082-8>, 2008.

16 Zhang, G. L., Zhang, J., Ren, J. L., Li, J. B., and Liu, S. M.: Distributions and sea-to-air fluxes of methane  
17 and nitrous oxide in the North East China Sea in summer, *Mar. Chem.*, 110, 42-55,  
18 <https://doi.org/10.1016/j.marchem.2008.02.005>, 2008.

19 Zhan, M. J., Sun, J. Y., Zhang, Y. M., Zhang, X. C., Nie, H., Deligeer, Kivekas, N., and Lihavainen, H.: The  
20 influence of air mass sources on the particle number concentration and the size distribution at Mt. Waliguan,  
21 *Journal of Glaciology and Geocryology*, 31, 659-663, 2009.

22 Zang, K. P., Zhao, H. D., Wang, J. Y., Xu, X. M., Huo, C., and Zheng, N.: High-resolution measurement of  
23 CH<sub>4</sub> in sea surface air based on cavity ring-down spectroscopy technique: the first trial in China Seas. *Acta*  
24 *Scientiae Circumstantiate*, 33, 1362-1366, 2013.

25 Zhang, F., Chen, Y. J., Tian, C. G., Wang, X. P., Huang, G. P., Fang, Y., and Zong, Zheng.: Identification and  
26 quantification of shipping emissions in Bohai Rim, China, *Sci Total Environ*, 497-498, 570-577,  
27 <https://doi.org/10.1016/j.scitotenv.2014.08.016>, 2014.

28 Zhai, W. D.: Sea surface partial pressure of CO<sub>2</sub> and its controls in the northern south China Sea in the non-  
29 bloom period in spring, *Haiyang Xuebao*, 37, 31-40, <https://doi.org/10.3969/j.issn.0253-4193.2015.06.004>, 2015.



1           Zhang, J. Y., Song, S. H., Xu, R., and Wen, J. H.: Source of airborne particulate matter in Guilin based on  
2 backward trajectory model, *Environmental Monitoring in China*, 33, 42-46, [https://10.19316/j.issn.1002-](https://10.19316/j.issn.1002-6002.2017.02.07)  
3 [6002.2017.02.07](https://10.19316/j.issn.1002-6002.2017.02.07), 2017.

4           Zang, K. P., Zhou, L. X., and Wang, J. Y.: Carbon Dioxide and Methane in the China Sea Shelf Boundary  
5 Layer observed by Cavity Ring-Down Spectroscopy, *J. Atmos. and Ocean. Tech.*, 34, 2233-2244,  
6 <https://doi.org/10.1175/JTECH-D-16-0217.1>, 2017.

7           Zhang, Z. P., and Chu, Z. X.: Modern variations in clay minerals in mud deposits of the Yellow and East  
8 China Seas and their geological significance, *Holocene*, 28, 386-395, <https://doi.org/10.1177/0959683617729446>,  
9 2018.

10          Zou, L., Hu, B., Li, J., Dou, Y. G., Xie, L. H., and Dong, L.: Middle Holocene Organic Carbon and biomarker  
11 records from the South Yellow Sea: relationship to the East Asian Monsoon, *J. Ocean Univ. China*, 17, 823-834,  
12 <https://doi.org/10.1007/s11802-018-3521-y>, 2018.

13          Zhang, Y., Deng, F., Man, H., Fu, M., Lv, Z., Xiao, Q., Jin, X., Liu, S., He, K., and Liu, H.: Compliance and  
14 port air quality features with respect to ship fuel switching regulation: a field observation campaign, SEISO-Bohai,  
15 *Atmos. Chem. Phys.*, 19, 4899–4916, <https://doi.org/10.5194/acp-19-4899-2019>, 2019.

16          Zang, K. P., Zhang, G., Xu, X. M., and Yao, Z. W.: Impact of air-sea exchange on the spatial distribution of  
17 atmospheric methane in the Dalian Bay and adjacent coastal area, China, *Chemosphere*, 251, 126412,  
18 <https://doi.org/10.1016/j.chemosphere.2020.126412>, 2020.

19

1

## **Author biography**



2

3

### **Kunpeng Zang**

4

Education experience:

5

2003-2007 Nanjing University of Information Science and Technology,  
6 undergraduate.

7

2007-2010 Chinese Academy of Meteorological Sciences, environmental  
8 engineering, Master.

9

2014-2018 Nanjing University of Information Science and Technology,  
10 Atmospheric Physics and Atmospheric Environment, Doctor.

11

Working experience:

12

2010-2020 National Marine Environmental Monitoring Center.

13

2020-now Zhejiang University of Technology, Lecturer.

14

Research field:

15

Greenhouse Gas observation research.

16



17

18

### **Shuangxi Fang**

19

Education experience:

20

1998-2003 Wuhan University, undergraduate.

1           2002-2007 Institute of Ecology and Environment, Chinese Academy of Sciences,  
2 Master Degree Candidate and Doctor.

3           Working experience:

4           2007-2015 Chinese Academy of Meteorological Sciences.

5           2015-2019 Meteorological Observation Center of China Meteorological  
6 Administration.

7           2019-now Zhejiang University of Technology, Professor.

8           2021-now Zhejiang Carbon Neutral Innovation Institute, Dean.

9           Research field:

10          Greenhouse Gas observation research.

11



12

13          **Jiaxin Li**

14          Education experience:

15          2016-2020 Heilongjiang University of Science and Technology, environmental  
16 engineering, undergraduate.

17          2020-2023 Zhejiang University of Technology, Master.

18          Research field:

19          Greenhouse Gas observation research.